J. Fluid Mech. (1979), *vol.* 93, *part* 3, *pp.* 413–432
Printed in Great Britain

The organized nature of flow impingement upon a corner

By D. ROCKWELL AND C. KNISELY
Department of Mechanical Engineering and Mechanics,
Lehigh University, Bethlehem, Pa. 18015, U.S.A.

(Received 1 June 1978)

Oscillations of impinging flows, which date back to the jet-edge phenomenon (Sondhaus 1854), have been observed for a wide variety of impingement configurations. However, alteration of the structure of the shear layer due to insertion of an impingement edge (or surface) and the mechanics of impingement of vortical structures upon an edge have remained largely uninvestigated. In this study, the impingement of a shear layer upon a cavity edge (or corner) is examined in detail. Water is used as a working fluid and laser anemometry and hydrogen bubble flow visualization are used to characterize the flow dynamics. Reynolds numbers (based on momentum thickness at separation) of 106 and 324 are employed. Without the edge, the shear layer produces the same sort of non-stationary (variable) velocity autocorrelations observed by Dimotakis & Brown (1976). When the edge is inserted, the organization of the flow is dramatically enhanced as evidenced by a decrease in variability of autocorrelations and appearance of well-defined peaks in the corresponding spectra. This enhanced organization is not locally confined to the region of the edge but extends along the entire length of the shear layer, thereby reinforcing the concept of disturbance feedback. Comparison of spectra with and without insertion of the edge reveals a remarkable similarity to those of a non-impinging shear layer with and without application of sound at a discrete frequency (Browand 1966; Miksad 1972); with enhanced organization at the fundamental frequency, simultaneous enhancement occurs also at the sub- and higher-harmonics.

Visualization of the vortical structures in the vicinity of the impingement edge shows that an impinging structure may experience one of three possible events: complete clipping, whereby the structure is swept down into the cavity; partial clipping, which results in severing of the vortex; or escape, involving deformation of the vortex while it is swept (intact) downstream past the edge. In general, no one of these events persisted continuously over a long period, but tended to occur alternately, meaning that 'jitter' of an impinging structure occurs. Plots of paths of these structures versus time showed that the convective speed of the vortex was locally influenced a distance of about four momentum thicknesses upstream of impingement, which is less than the estimated diameter of an impinging vortical structure. Furthermore, this upstream influence of the edge is also evident in the distributions of transverse velocity. Laser measurements indicate that the presence of the edge substantially increases the local value of transverse velocity fluctuation in the region immediately upstream of the edge.

0022-1120/79/4271-7000 $02.00

1. Introduction

The unsteady nature of free shear layers that impinge upon solid boundaries has received considerable attention in recent years, motivated by applications in the areas of noise generation and structural loading. Among the diverse configurations which have produced organized oscillations are the jet-edge (Powell 1961; Karamcheti *et al.* 1969), cavity-edge (Sarohia 1977), and mixing-layer-wedge (Hussain & Zaman 1978). Despite differences in shear layer and impingement edge geometry of these flows, they exhibit several common characteristics, suggesting that the same underlying flow mechanisms sustain the oscillations. Yet, as pointed out in the review of Rockwell & Naudascher (1978), there remain some central questions which must be addressed if an understanding of the self-sustaining mechanisms is to be achieved. Perhaps the most important of these is the manner in which an impingement edge influences the organization of the shear layer and to what extent the energy concentration at the fundamental, harmonic, and subharmonic frequencies is altered. Closely associated with this influence of the edge is the deformation of vortical structures in the vicinity of the edge. Such interaction is important from two perspectives: the unsteady structural loading of the edge and its support and the generation of pressure perturbations which are propagated upstream and disturb the free shear-layer near its origin. This study focuses on these, as yet, uninvestigated features of vortex-edge interaction and the influence of the edge on the evolution of the upstream shear layer.

It is well known that non-impinging shear layers which are transitional or turbulent have an organized structure. Summaries of advances in this area are given by Winant & Browand (1974), Davies & Yule (1975) and Roshko (1976). Associated with this coherent nature of the flow is a 'jitter', or irregularity, in the growth and amalgamation of the vortical structures. Although the source of this 'jitter' has not been resolved. it seems to be due, at least in part, to the overall nature of the flow, as advanced by Dimotakis & Brown (1976). They hypothesize, on the basis of autocorrelation measurements, that a non-impinging shear layer is influenced by the dynamics of the flow downstream of a given station. Since the strength of a vortical structure increases with downstream distance, even structures at large distances exert an upstream influence in accordance with the Biot–Savart Law. A consequence of this upstream modulation was variability in autocorrelation functions measured at locations just downstream of separation. Although their experiments were carried out at a high Reynolds number, the essential features of growth and interaction of coherent structures have been shown to persist over a wide range of Reynolds number (Winant & Browand 1974; Browand & Weidman 1976).

In this study, a direct comparison of a separated shear layer with and without an impingement edge was undertaken. To avoid misleading effects associated with possible occurrence of standing waves in air flows (Rockwell & Naudascher 1978, 1979), water was used as the working fluid. Extensive hydrogen bubble visualization of the flow and accompanying laser–Doppler measurements in the vicinity of the impingement edge allowed identification of several mechanisms associated with vortical structure-edge interaction. In addition, the effect of the edge is shown, by comparison of autocorrelations and spectra, to be a global one; the growth of the fundamental, subharmonic, and three-halves harmonic components is dramatically altered over the entire length of the shear layer. This overall effect is remarkably

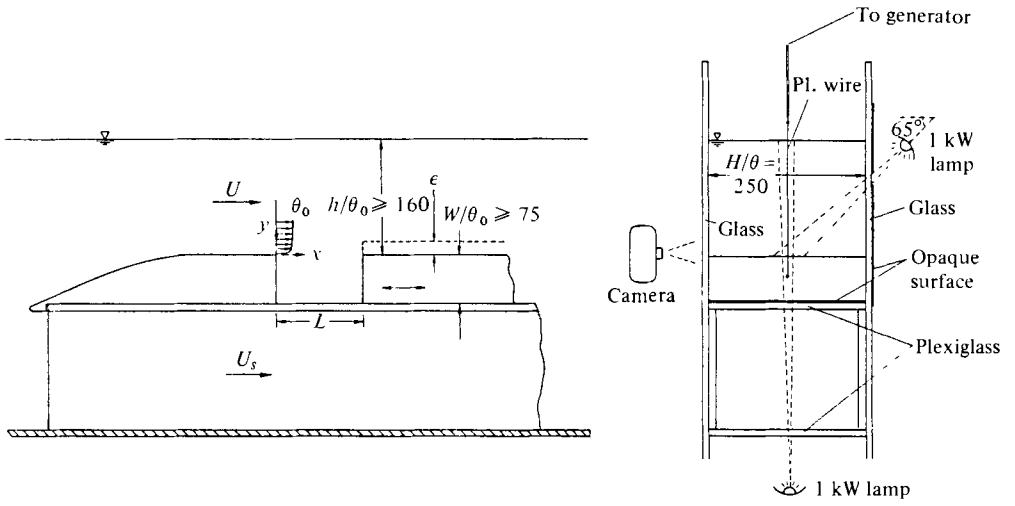

FIGURE 1. Overall view of test section illustrating adjustable cavity and lighting arrangement for hydrogen bubbles.

similar to exciting a non-impinging free shear layer at its fundamental frequency; energy becomes sharply concentrated not only at the fundamental but also at its harmonics. The implication is that the upstream propagation of pressure disturbances from the edge to the separation region is essentially equivalent to applying disturbances at a discrete frequency.

2. Experimental system and instrumentation

A water channel, with appropriate flow straighteners and screens in its upstream plenum chamber, housed the cavity flow apparatus shown in figure 1. To provide a well-defined boundary layer at separation, the incident flow was divided into two streams, one passing beneath the rig and the other experiencing acceleration prior to separation at the upstream cavity edge. The ratio of the flow rate of these two streams, and consequently the location of the stagnation point at the leading edge of the cavity apparatus, was adjusted by a flap arrangement at the downstream end of the channel test section. Water depth in the channel was maintained at least a height of 160 momentum thicknesses above the separation edge of the cavity to insure a uniform stream of substantial extent. At the flow velocities investigated in this study, only very small amplitude perturbations existed at the free surface; nevertheless, detailed spectral measurements (using a logarithmic amplitude scale) were taken in the free stream at locations upstream and downstream of separation, and in the boundary layer at separation. These spectra showed no discernable contributions from either surface ripples or undesirable upstream effects.

Flow visualization was achieved using the hydrogen bubble technique, involving a vertical wire mounted at an axial location just downstream of separation. In addition to lighting at an angle of about 65° with respect to the bubble sheet (see figure 1), as is typically the case, it was necessary to provide lighting in the plane of the sheet emanating from beneath the channel test section. The location and width of the

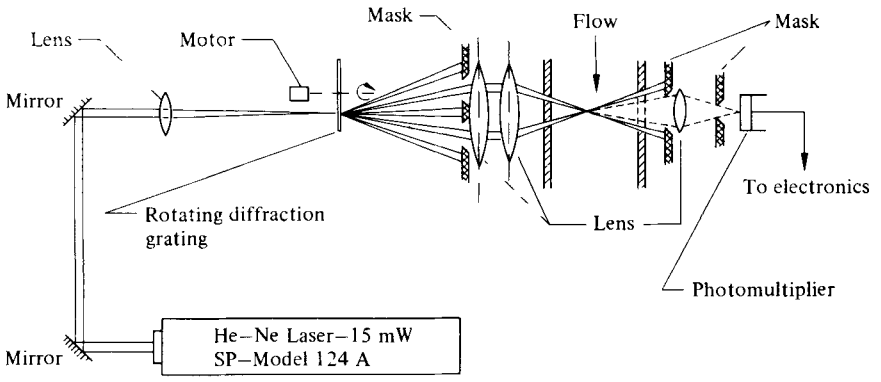

FIGURE 2. Schematic diagram of laser–Doppler anemometer system.

corresponding light collimation slits on the bottom and the sides of the test section was also critical. In visualizing recirculating cavity flows, care must be taken to avoid excessive build-up of recirculating bubbles in the cavity which eventually obscures the view of the shear layer. Another complication is bubble rise from the low velocity region of the cavity up to the shear layer. To minimize these difficulties, it was necessary to design a probe holder for the platinum wire which could be adjusted vertically at any streamwise position, and to adjust the vertical position of the probe until the lower end of the generating wire was within a sufficiently high velocity portion of the shear layer.

Laser–Doppler anemometry allowed accurate measurement of mean and time-dependent velocity components in regions of streamline curvature and relatively high turbulence intensity, which became particularly acute in the vicinity of the impingement edge. As shown in figure 2, a 15 mW He–Ne (Spectra-Physics) laser was employed in the forward scatter fringe mode. A rotating diffraction grating served as a beam splitter as well as a mechanical frequency shifter (Durst, Melling & Whitelaw 1976). All optics were mounted on a traversing mechanism that allowed adjustment in three orthogonal directions. The output from the tracker could be processed through a d.c. voltmeter, r.m.s. voltmeter, a Fourier analyser for spectral analysis, or an XY plotter for traverses.

3. Mean flow conditions

After considering both time averaging and visualization requirements, it was decided to employ two values of Reynolds number based on momentum thickness at separation (Re_{θ_0} = 106, 324). Corresponding values of dimensionless momentum thickness were θ_0/W = 0·014 and 0·008, where W = 7·4 cm. The lower value allowed detailed hydrogen bubble visualization, while the higher permitted use of much shorter time constants and sampling intervals during laser measurements. The shape factor of the velocity distribution at separation δ_0^*/θ_0 was 2·52 ($\pm$ 0·11). A typical family of velocity distributions, corresponding to the higher speed flow, is depicted in figure 3.

At each of the two Reynolds numbers examined herein, a sufficiently long cavity length was chosen to allow development of the shear layer disturbance well into the nonlinear regime (Browand 1966; Miksad 1972). The corresponding Reynolds numbers based on cavity length L were $1{\cdot}9 \times 10^4$ and $4{\cdot}6 \times 10^4$. To ascertain that these cavity

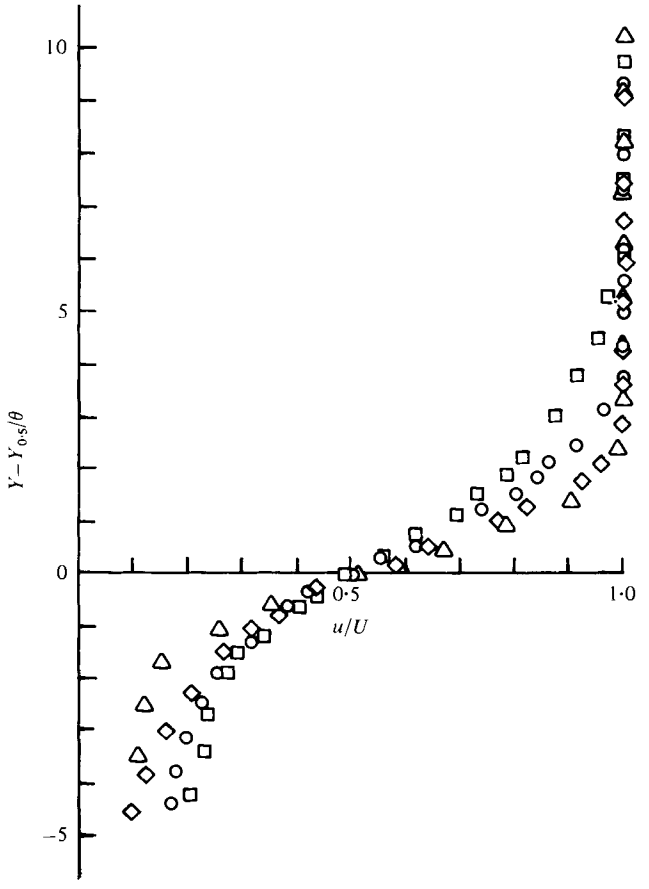

FIGURE 3. Typical series of mean velocity distributions taken in the cavity shear layer $Re_{\theta_0} = 324$, $L/\theta_0 = 144$. x/θ_0 values: △, 36; ◇, 71; ○, 107; □, 134.

lengths did not correspond to conditions at or near a frequency 'jump', which typically occurs in impinging flows (Rockwell & Naudascher 1979), impingement wall pressure spectra were acquired for a range of cavity lengths. These spectra show that the chosen cavity lengths lie in the centre of a stage of oscillation, and each of the cavity lengths corresponds to approximately three and one-half wavelengths of the most amplified disturbance in the shear layer. According to Sarohia (1977), cavity depth can be a significant parameter in determining the onset of oscillation if the ratio of boundary layer thickness to depth δ_0/W is greater than approximately 0·5. In this study, corresponding ratios were $\delta_0/W = 0{\cdot}088$ and 0·130.

Two-dimensionality of the velocity field at separation was measured by traversing the laser system in the spanwise direction at a given distance from the wall y. The velocity at several values of y in the boundary layer and in the free stream was uniform within 1% of the corresponding midplane value except for the end-wall region. Extent of the end-wall boundary layer, defined as the ratio of displacement thickness to half-channel width $\delta_w^*/\frac{1}{2}H$, was of the order of 5×10^{-2}. Furthermore, the ratio of channel span to separation momentum thickness (H/θ_0) was $\simeq 400$.

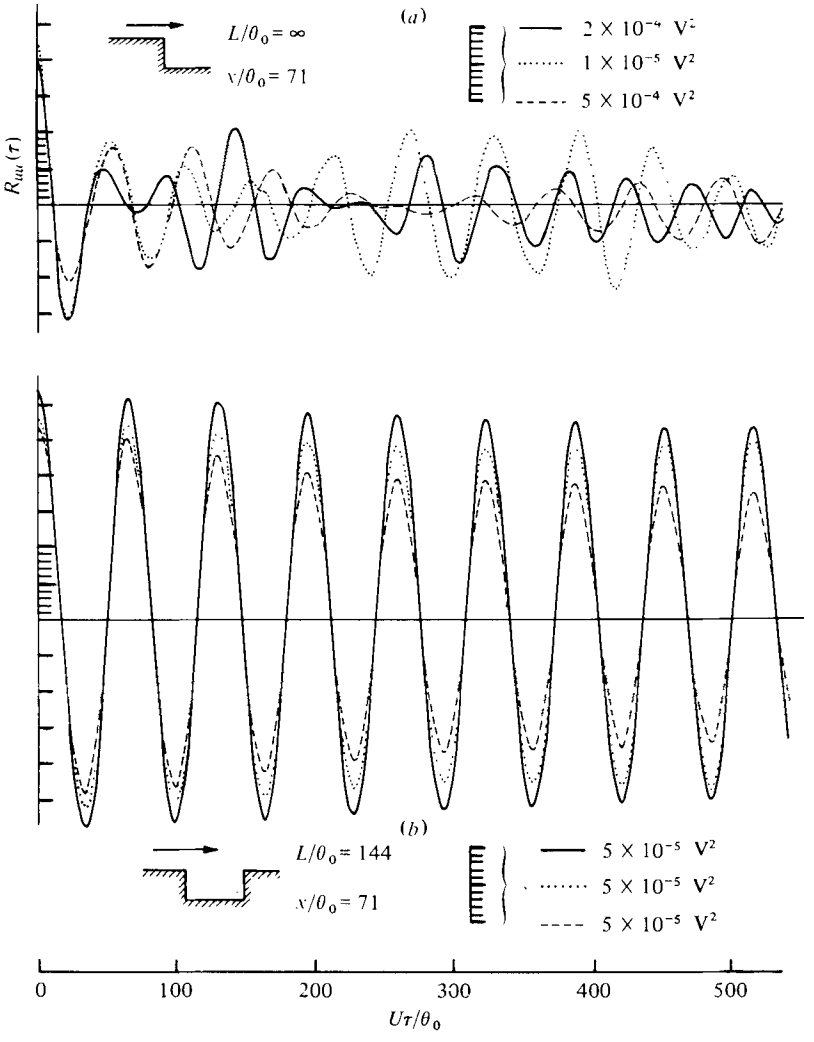

FIGURE 4. For legend see facing page.

4. Organization of flow due to impingement edge

Although the coherent structure of mixing layers in the absence of impingement edges is well documented for a wide range of Reynolds number (Winant & Browand 1974; Roshko 1976), large variability in the organization of the mixing layer can occur, as strikingly evidenced by the autocorrelations of Dimotakis & Brown (1976). The non-congruency of these autocorrelations taken at the same location in the mixing layer, but at different times, led them to postulate a coupling between the downstream and upstream dynamics of the flow. In other words, there exists a feedback mechanism in the form of upstream disturbance propagation. If there is indeed such a feedback mechanism, it would seem that insertion of an impingement edge could enhance the strength of the fed back disturbance, thereby increasing the degree of organization of the shear layer dynamics.

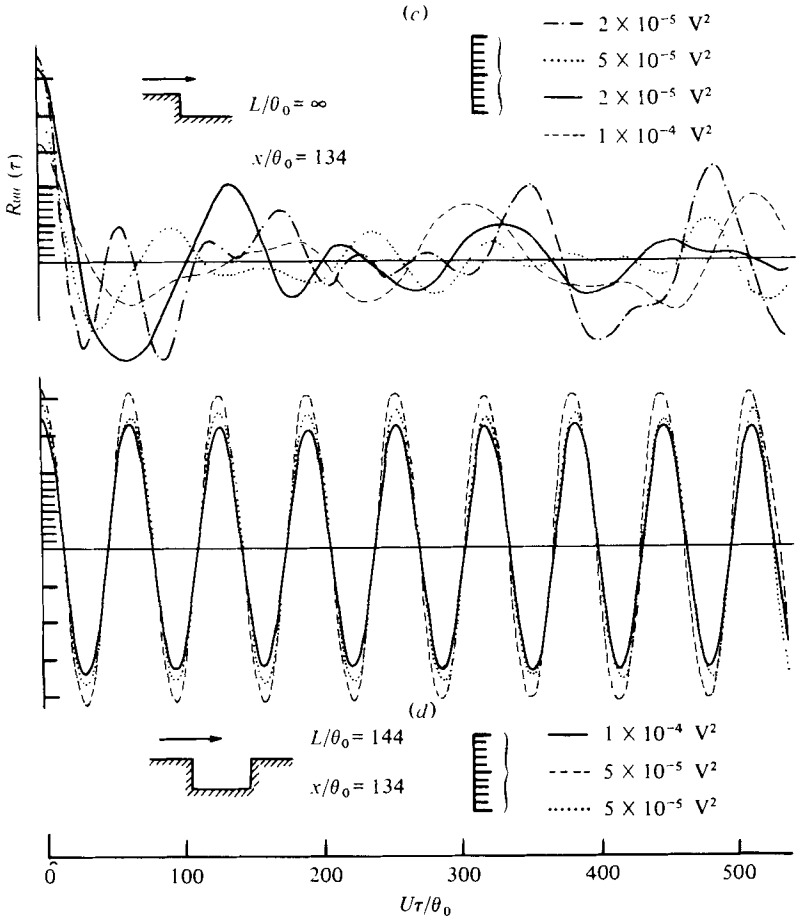

FIGURE 4. Comparison of autocorrelations taken with and without the cavity impingement edge at corresponding locations in the cavity shear layer ($u/U = 0{\cdot}95$).

With this hypothesis in mind, examination of the unsteady nature of the shear layer with and without the downstream edge of the cavity was carried out (see figure 4). As in the study of Dimotakis & Brown, autocorrelations were taken along the edge of the shear layer at locations corresponding to $u/U = 0{\cdot}95$. Each autocorrelation trace shown in figure 4 represents the average of six sequential samples (35 oscillation cycles per sample); furthermore, the time between each trace (~ 800 oscillation cycles) was maintained constant. For the case of no impingement edge, there are indeed large variabilities of the autocorrelations similar to those measured by Dimotakis & Brown. The typical period of oscillation, though quite irregular, is longer at the larger streamwise distance, implying occurrence of vortex pairing. Maintaining essentially the same sampling conditions and interval between correlation runs, autocorrelations were acquired with the impingement edge in place. The enhanced organization of the flow is indeed dramatic, with undetectable variations in frequency of oscillation. Furthermore, the similarity of the autocorrelations at $x/\theta_0 = 71$ and 134 suggests that the organization persists along the entire length of the cavity shear layer. Evidence of this *global nature of the enhanced organization* of the

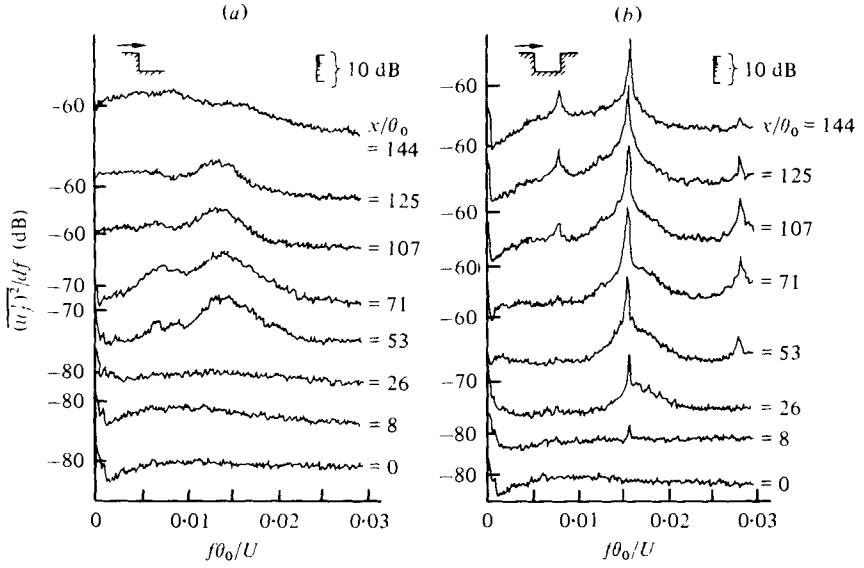

FIGURE 5. Comparison of streamwise evolution of velocity spectra with and without the cavity impingement edge at corresponding locations in the cavity shear layer ($u/U = 0{\cdot}95$).

shear layer is exhibited in figure 5, which shows a direct comparison of spectra without and with the impingement edge. The concentration of energy at the fundamental frequency β is much stronger in presence of the edge, and the amplitude of the fundamental overshadows the amplitudes of the sub- and first harmonics $\frac{1}{2}\beta$, 2β along the entire length of the shear layer. For the case of no impingement edge, the amplitude of the subharmonic $\frac{1}{2}\beta$ is barely discernable, and there is no evidence of the first harmonic 2β. Amplitude variations are plotted as a function of streamwise distance in figure 6; all amplitudes are normalized with respect to the maximum amplitude of the fundamental β in presence of the edge. On the basis of this plot, and the spectra of figure 5, it may be concluded that the effect of the impingement edge is not simply an enhanced organization at the fundamental frequency, but also at the harmonic and subharmonic frequencies. As a result, the growth rates of all components are influenced. Clearly, *the spectral evolution of an impinging shear layer cannot be deduced from that of the corresponding non-impinging shear layer even at large distances upstream of impingement.*

In a series of experiments in the absence of an impingement edge, Browand (1966) and Miksad (1972) demonstrated that application of sound at the fundamental frequency yielded a substantial increase in organization of the flow at the fundamental and its harmonics and subharmonic. Comparison of their spectra with those of figure 5 reveals a remarkably similar influence of externally applied sound and insertion of an impingement edge. This similarity reinforces the concept of disturbance feedback, whereby continuous communication between the impingement edge and the sensitive region of the shear layer near separation promotes a globally organized oscillation. Although the precise details of this feedback mechanism are still not clearly resolved (Rockwell & Naudascher 1979), a plausible explanation is that pressure fluctuations, arising from impingement of vortical structures at the edge, are propagated upstream to the region of 'maximum receptivity' near shear layer separation.

This global influence on the spectral evolution of the shear layer due to the impinge-

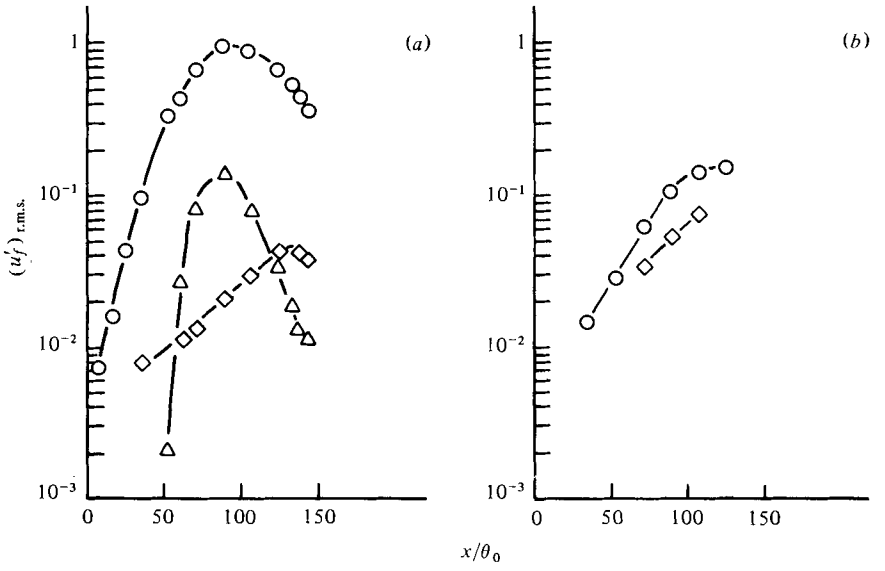

FIGURE 6. Growth of amplitudes of fundamental β, first harmonic 2β, and subharmonic $\frac{1}{2}\beta$ corresponding to spectra of figure 5, with and without cavity impingement edge. ○, β; △, 2β; ◇, $\frac{1}{2}\beta$. (*a*) $L/\theta_0 = 144$; (*b*) $L/\theta_0 = \infty$.

ment edge is tied to the development of the mean flow along the entire length of the shear layer. Indeed, Sarohia (1977) has found that the growth rate of mean momentum thickness is a function of cavity length. In view of the drastic alteration of the unsteady flow character shown here, it is most likely that the change in mean growth rate is achieved through modification of the Reynolds stress distribution within the shear layer.

5. Impingement region

In order to examine in detail the effect of the impingement edge on organization of the flow, hydrogen bubble visualization was undertaken. The flow conditions and cavity length were chosen to provide a well-defined vortex just upstream of impingement. Spectra of the corresponding velocity and pressure fluctuations near impingement showed that contributions to the kinetic energy from frequencies other than the fundamental were very small, and that the cavity length was approximately equal to three and one-half disturbance wavelengths. As shown in figure 7 (plate 1), for the same mean flow conditions and cavity geometry, one of several possible events may occur as a typical vortex (figure 7*a*) approaches the impingement edge: complete 'clipping' of the vortex whereby the entire structure is swept downwards (figure 7*b*); partial clipping that severs the vortex into a component swept downwards and a component convected downstream (figure 7*c*); and 'escape', in which case the vortex is not clipped but retains its integrity and continues downstream (figure 7*d*)†. Also shown at exactly the same axial location is the corresponding flow without an impingement edge (figure 7*e*). In this case, vortex pairing occurred upstream of this location, and the flow was, in general, less organized. These observations of enhanced organization in the presence of the impingement edge (figures 7*a–d*) are reflected in the autocorrelations and spectral distributions of figures 4 and 5.

† See note added in proof.

The variability of possible events shown in figure 7*b–d* may be termed 'jitter'. That is, although the impingement edge greatly enhances the organization of the flow and yields averaged autocorrelations (figure 4) having undetectable variations in frequency, these same autocorrelations exhibit a noticeable jitter in amplitude. Further details of this jitter in the presence of an impingement edge are displayed in figure 8 (plate 2). In both photos, the large-scale downstream vortices have escaped clipping, and are shown at the same axial location. Yet, the upstream nascent vortices exhibit a different degree of maturity even though the wavelength between vortices appears to be the same. In contrast to this jitter in amplitude, it appears, from the autocorrelations of figure 4, that the corresponding non-impinging shear layer exhibits both frequency and amplitude jitter. This sort of variability has been reported in other investigations of non-impinging shear layers (Rockwell & Niccolls 1972; Winant & Browand 1974; Roshko 1976). There are, of course, several features of the flow that may influence jitter in both cases – with and without the impingement edge: low frequency modulation of the shear layer near separation by the dynamics of the adjacent recirculation zone of the cavity (Chandrsuda *et al.* 1978); three-dimensional effects, which are inevitable in the nonlinear region of disturbance growth (Miksad 1972; Rockwell & Knisely 1979; Konrad 1976); and end wall effects, which can exert substantial spanwise influence (Holdeman & Foss 1975; Rockwell 1976).

Additional aspects of the complete clipping process are illustrated in figure 9 (plate 2). Even though the structure is essentially severed, an elongated pocket of vorticity forms downstream of the edge. Associated with this process is acceleration of the flow (i.e. increased distance between timelines) at the upper edge of the pocket. In the event that the cavity length is half that for the flows corresponding to figures 7–9, no discrete vortex is formed, as shown in figure 10 (plate 2). This is due to the inhibited streamwise growth of the shear-layer disturbance (due to the short streamwise length scale), and the consequently small disturbance feedback. The hot wire measurements of Sarohia (1977) show the existence of a certain minimum cavity length (for given initial conditions) above which oscillations will be self-sustaining. It would appear that the case illustrated in figure 10 corresponds to the cavity length at which oscillations are first detectable.

The probability of occurrence of each of the events of figures 7 (*b–d*) depended upon the vertical displacement of the impingement edge ϵ, defined in figure 1. For negative values of ϵ, the probability of escape was high, whereas for positive values of ϵ, the probability of partial clipping was high. Over the range of ϵ examined in this study, complete clipping occurred infrequently. These possible fates of a vortex approaching the edge are tied to the time mean pattern of the flow. Since the time-mean volume defined by the cavity and shear-layer is a closed one, location of the mean stagnation-streamline tended to shift with changes in ϵ, as verified by laser measurements. By artificially adding or removing mass to or from the cavity, it should be possible to control the location of the mean stagnation streamline and induce more consistent escape or complete clipping. In turn, it would be possible to control the pressure fluctuations at the cavity impingement edge. Sarohia & Massier (1977) have indeed shown that the amplitude of cavity oscillations can be substantially reduced via mass addition.

Further insight into the vortex-edge interaction can be gained by examining sequential photos extracted from 16 mm films. Figures 11 and 12 (plates 3 and 4)

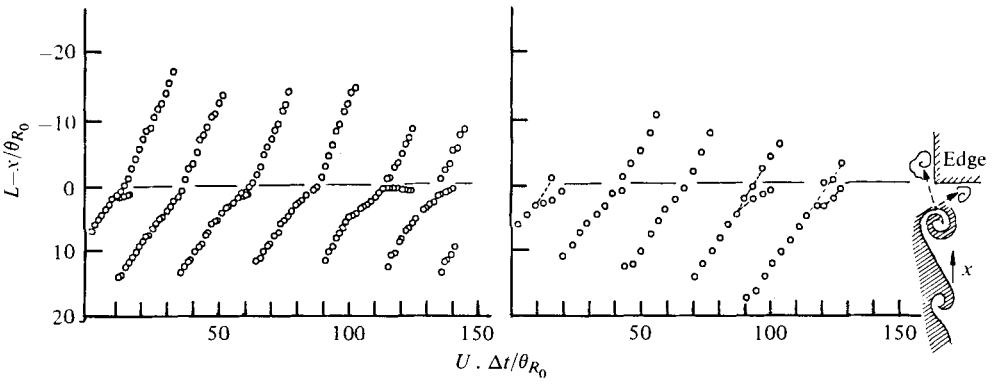

FIGURE 14. Variation of vortex position $(L-x)/\theta_{R_0}$ as a function of time Ut/θ_{R_0} for two extreme values of edge height ϵ/θ_{R_0}. (*a*) $\epsilon/\theta_{R_0} = 6{\cdot}25$; (*b*) $\epsilon/\theta_{R_0} = 0$.

portray the process of partial clipping for two different values of corner displacement ϵ. In figure 11, the incident vortex is clipped below its centre, while in figure 12, it is clipped above its centre. For both cases, the portion of the vortex that is transported downstream experiences substantial distortion in the streamwise direction. Clearly, this is associated with shearing of the original vortex in two directions – one downward into the cavity and the other downstream. In the case of the vortex of figure 11, the portion swept downstream exhibits a well-defined coherence and larger scale than shown in figure 12. The transverse location ϵ of the impingement edge in the mean shear layer differs by only three momentum thicknesses (i.e. $\epsilon = 0$ and $3{\cdot}12\,\theta_{R_0}$, respectively) for these two series. Yet, the difference in scale of the vortex swept downstream past the corner is clearly distinguishable. The fact that the above-described 'jitter' effect can result in escape of the impinging vortex, even at larger values of corner displacement ($\epsilon/\theta_{R_0} = 3{\cdot}12$), is portrayed in figure 13 (plate 5). After negotiating the corner, the vortex experiences distortion in the streamwise direction and eventual breakdown.

The influence of the impingement edge on the paths of the vortices is illustrated in figure 14. These paths were obtained from frame by frame analysis of 16 mm films, originally taken at speeds of 12 and 32 frames per second. Two continuous series, corresponding to $\epsilon/\theta_{R_0} = 0$ and $6{\cdot}25$, show cases of partial clipping and escape of the incident vortices. At distances sufficiently far upstream of the edge, the convective speed of the vortices is essentially constant. Moreover, it is evident that vortex pairing does not occur upstream of the edge. As the edge is approached the velocity of the vortices decreases; in cases where partial clipping occurs, this decrease is quite substantial. Downstream of the edge, the convective speed is also essentially constant. In some cases, the centres of vortices became indiscernable shortly after negotiating the edge. Due to this uncertainty, corresponding points were not included in figure 14. It appears that, in general the convective velocity of the vortices is not influenced for distances upstream of the edge greater than $4\theta_{R_0}$. Since the estimated scale of a typical vortex is $6\theta_{R_0}$, this means that the influence of the edge on the convective velocity is negligible for distances less than a vortex diameter. Of course, the vorticity distribution of the incident vortex and the shape of the impingement corner, or surface, will play a strong role in determining the extent of upstream influence.

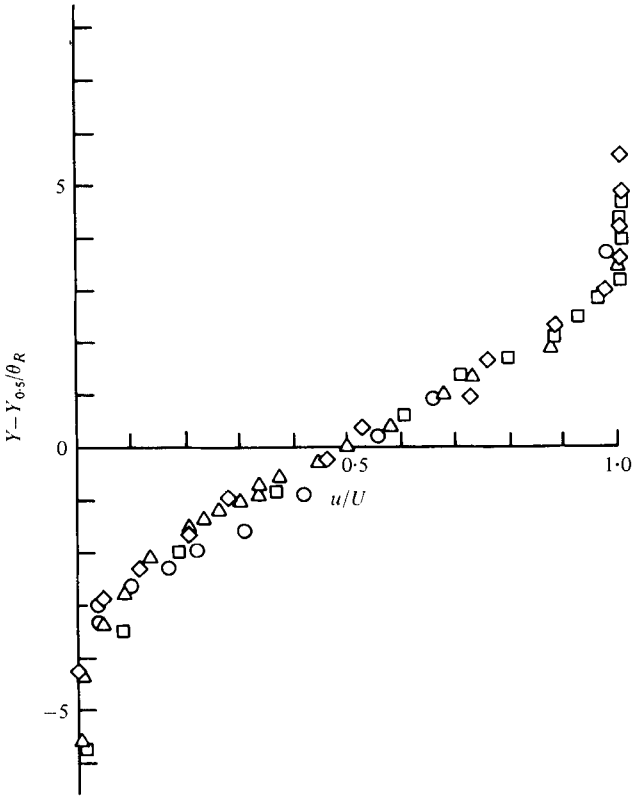

FIGURE 15. Distributions of mean velocity u for various heights of the downstream cavity edge ϵ. $Re_{\theta_0} = 106$, $L/\theta_0 = 142$, $x/L = 0{\cdot}96$. Values of ϵ/θ_{R_0} are: □, 6·25; ◇, 3·12; △, 0; ○, −3·12.

Detailed laser measurements of the mean and fluctuating velocity field were carried out in the vicinity of the impingement edge. In order to provide a suitable length scale for this region, a reference momentum thickness (θ_R) was defined upstream of the impingement edge at $x/\theta_0 = 136$. In general, θ_R is a function of ϵ; it is designated as θ_{R_0} at $\epsilon = 0$. Mean velocity distributions taken at this axial location for four different values of ϵ can be approximated by a single distribution when θ_R is used as the characteristic length for normalization (see figure 15). Distributions of the transverse velocity fluctuations ($v_{\text{r.m.s.}}$) immediately upstream of the impingement edge can be measured best with a frequency-shifted laser system because the mean component ($\bar{v}$) passes through zero when the shear layer is traversed. The family of $v_{\text{r.m.s.}}$ distributions illustrated in figure 16 shows that the maximum of each distribution is shifted approximately the same distance as ϵ if ϵ is positive, while there is substantial difference if ϵ is negative. Moreover, the maximum amplitude of $v_{\text{r.m.s.}}$ decreases as ϵ increases. This dependence of amplitude on ϵ is related to the scale of the impinging vortex. Study of films for $\epsilon = 6{\cdot}25\ \theta_{R_0}$ and $-3{\cdot}12\ \theta_{R_0}$ revealed that vortices were somewhat more mature (larger scale) for the latter case; in addition, vortex pairing sometimes occurred for the latter, but never for the former.

Using the local momentum thickness θ_R as a normalizing length, the variations of $v_{\text{r.m.s.}}$ are seen to collapse approximately to a single distribution, as illustrated in

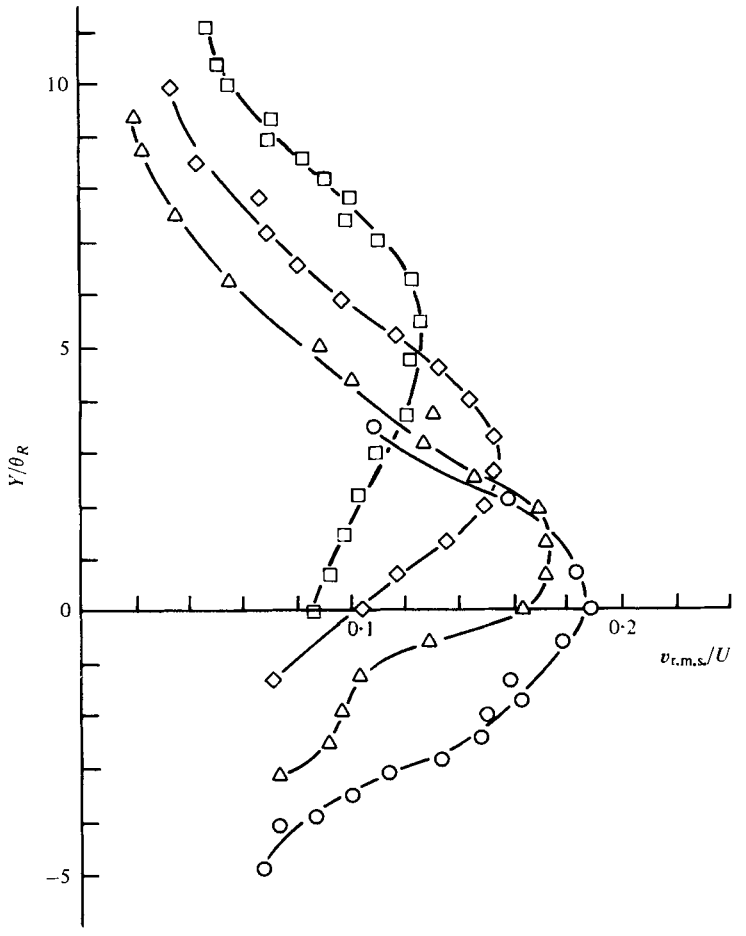

FIGURE 16. Distributions of transverse velocity fluctuation $v_{r.m.s.}$ as a function of height of downstream cavity edge. $Re_{\theta_0} = 106$, $L/\theta_0 = 142$, $x/L = 0{\cdot}96$. Symbols as in figure 15.

figure 17. A comparison of $v_{r.m.s.}$ distributions deduced from linear stability theory with the experimental distributions is given in figure 17. In determining these theoretical distributions, the real and imaginary eigenfunctions of Michalke's (1965) spatial theory were used. Qualitatively, the agreement is good in that the shape and symmetry of the distributions are approximated quite well. However, quantitatively, the (time-averaged) width of the experimental distribution exceeds that of the theoretical. This is due not only to application of the linear assumption in the far nonlinear regime, but also to the occurrence of vortex 'jitter'. Analogous comparisons have been made for the $u_{r.m.s.}$ distributions in non-impinging (Freymuth 1965) and impinging (Hussain & Zaman 1978) flows, and it has been shown that the widths of the experimental $u_{r.m.s.}$ distributions substantially exceeds those of the corresponding theoretical ones in the nonlinear region of the disturbance growth. In view of non-linearity, the vortex model of Stuart (1967) is more appropriate.

Browand & Weidman (1976) have simulated the consequence of vortex pairing on $u_{r.m.s.}$ and $v_{r.m.s.}$ distributions by using two sets of Stuart (1967) vortices, each having

a different longitudinal spacing. These sets (rows) occupied mutually exclusive fractions of the time record; furthermore, the vortex centres were displaced in the transverse direction with a defined probability distribution. So, for the most part, this model can be viewed as an effective simulation of 'jitter'; indeed, the distribution of $v_{\text{r.m.s.}}$ resulting from their model (figure 17) is significantly wider than that corresponding to the lowest frequency ($\beta = 0{\cdot}2$) of the linearized analysis.

As pointed out in the survey of Rockwell & Naudascher (1979), knowledge of the mass exchange in the vicinity of the impingement edge is essential to gaining an understanding of the mechanism which sustains cavity-type oscillations. Indeed, Heller & Bliss (1975) have visually related upstream wave propagation to what they presumed to be mass exchange near the impingement edge of a high Mach number cavity flow. However, no quantitative amplitude or phase measurements were carried out. Rigorously speaking, instantaneous streamlines are required to characterize the mass exchange near the trailing edge. Construction of such streamlines involves measuring the u and v components (amplitude *and* phase) throughout the domain of the impingement edge. In this investigation, the mass exchange in the transverse direction was characterized by measuring the distribution of $v_{\text{r.m.s.}}$, whose energy was primarily concentrated at the fundamental frequency of instability. These measurements were carried out along the line $y = 0$ near the impingement edge. For the case $\epsilon = 0$, for example, the ratio of the mean transverse velocity to the free stream velocity ($\bar{v}/U$) was less than 0·015 along the line $y = 0$, so the distributions of $v_{\text{r.m.s}}$ well represent amplitudes of instantaneous mass flux into and out of the cavity. As shown in figure 18, the shape of these distributions is essentially the same for $\epsilon/\theta_{R_0} = 0$, 3·12; the value of $v_{\text{r.m.s.}}$ increases rapidly as the impingement edge is approached and exhibits two maxima. One maximum is very close to the edge, and the other a distance upstream if the edge which is approximately equal to the scale of the vortex approaching impingement – this scale being estimated from the previously described flow visualization (i.e. figure 7). Also shown in figure 18 is a typical power spectrum; the predominance of the fundamental, β, is evident. Attempts were made to measure the distributions of $v_{\text{r.m.s.}}/U$ corresponding to the case of no impingement edge, thereby providing a direct comparison with the data of figure 18. But, as shown in figure 5, the edge globally influences the flow; consequently, such a comparison is meaningless. Examination of the photos of figures 12 and 13, which represent the case $\epsilon/\theta_{R_0} = 3{\cdot}12$, reveals that the mechanisms of clipping and escape of incident vortices are associated with the locally large transverse fluctuations in the vicinity of the edge. For extreme values of edge displacement ($\epsilon/\theta_{R_0} = -3{\cdot}12$, 6·25) the mean transverse velocity $\bar{v}$ is significant, so a direct comparison with figure 18 is not appropriate. Although not shown here, qualitatively similar variations of $v_{\text{r.m.s.}}/U$ *vs.* $(L-x)/\theta_{R_0}$ were obtained; amplitude saturation occurred substantially closer to the edge than for the cases illustrated in figure 18. Bearman (1972) has observed, for the case of a stagnation flow with upstream turbulence grids, an increase in the transverse fluctuation component $v_{\text{r.m.s.}}$ in the immediate vicinity of the impingement surface. However, the primary mechanism for the increase in his experiment involves vorticity amplification, rather than the type of vortex-edge interaction demonstrated in figures 12 and 13.

In order to construct profiles of the transverse fluctuation component v, at various values of time t of oscillation, it is necessary to know both the amplitude (see figure 18)

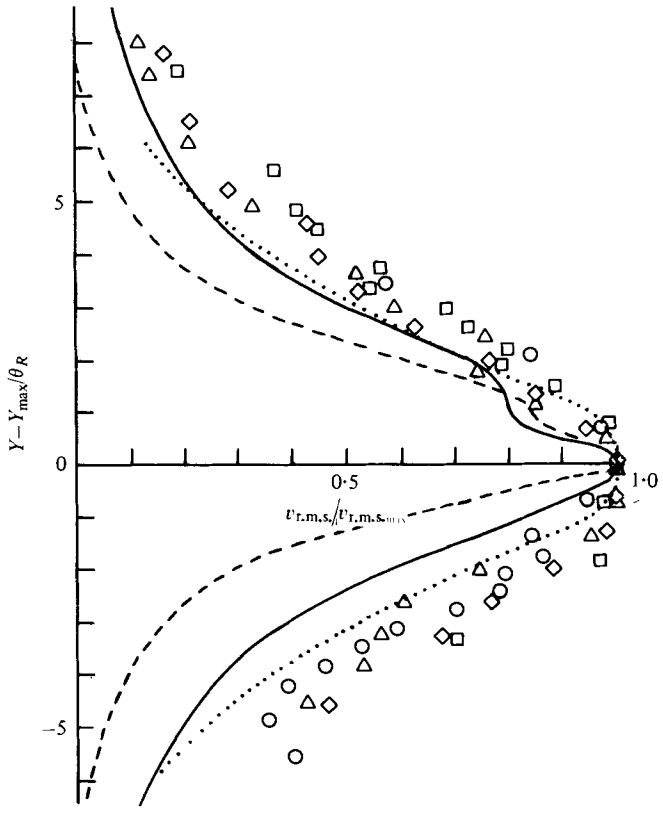

FIGURE 17. Comparison of theoretical and experimental distributions of fluctuating velocity $v_{\text{r.m.s.}}$. Theories: —— ($\beta = 0{\cdot}2$) and – – – ($\beta = 0{\cdot}3$) after Michalke (1965); . . ., Browand & Weidman (1976). $Re_{\theta_0} = 106$, $L/\theta_0 = 142$, $\theta = \frac{1}{2}(\theta_0 + \theta_{R_0})$. Symbols as in figure 15. $\beta_\theta = 0{\cdot}28$.

and phase distributions in the streamwise direction. This variation of phase was measured via a cross-correlation technique. Using the output of a pressure transducer mounted on the impingement wall as a reference, cross-correlations were taken with the laser signal to obtain the variation of phase along the mouth ($y = 0$) of the cavity. The resultant profiles are depicted in figure 19 for six values of dimensionless time (t/τ). These plots portray the sinusoidal mass flux into and out of the cavity in the vicinity of the impingement edge. It is evident that there is a strong phase variation of this mass exchange in the streamwise direction. In fact, the half-wavelength of these distributions is about $(L-x)/\theta_{R_0} \simeq 6{\cdot}5$; this value well approximates the half-wavelength between vortices measured from the photos of figure 11. However, there is substantial distortion of the distributions (indicated by the shaded symbols) for a distance of about $4\theta_{R_0}$ upstream of the impingement corner. This extent of upstream distortion is essentially the same as revealed in the plot of vortex trajectories (figure 14). Furthermore, for distances upstream of the corner greater than $15\theta_{R_0}$, distortion is again evident; in this case, it is due to the extremely low amplitude of $v_{\text{r.m.s.}}$. Since figure 11 shows that the mechanism which produces these transverse fluctuations is the streamwise convection and eventual impingement of the vortical structures upon the edge, a comparison with the non-impinging vortex model of Stuart is in order.

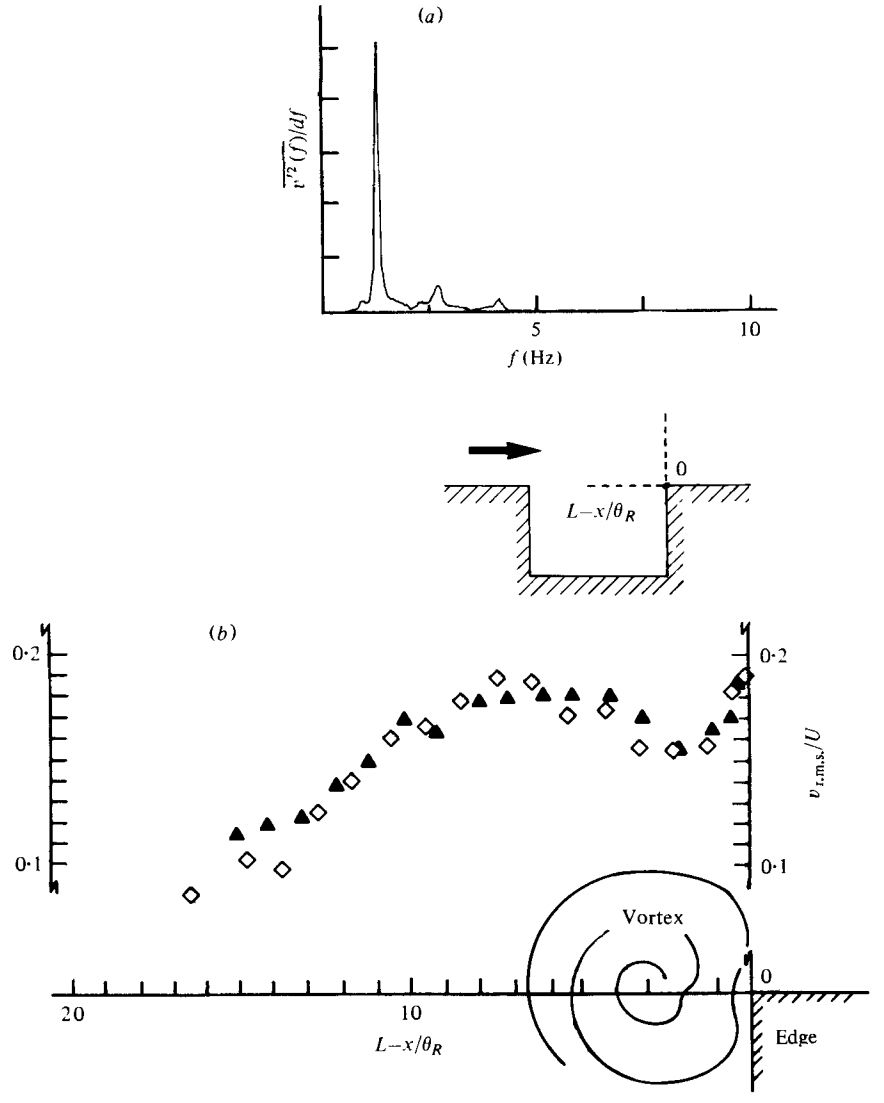

FIGURE 18. Variation of amplitude of transverse velocity fluctuation $v_{r.m.s.}$ as a function of distance from impingement edge $L-x$ and height of edge ϵ. Vortex drawn to scale. Typical power spectrum illustrates predominance of fundamental component. $Re_{\theta_0} = 106$, $L/\theta_0 = 142$. (*a*) $(L-x)/\theta_{R_0} = 1{\cdot}88$, $y = 0$, (*b*) $\diamond$, $\epsilon/\theta_{R_0} = 3{\cdot}12$; $\blacktriangle$, $\epsilon/\theta_{R_0} = 0$.

According to this model, the transverse velocity component corresponding to a row of vortices convected in the streamwise direction is:

$$v' = \frac{\Gamma}{2\lambda} \frac{\alpha \sin\left(\dfrac{2\pi x}{\lambda}\right)}{\cosh\left(\dfrac{2\pi y}{\lambda}\right) - \alpha \cos\left(\dfrac{2\pi x}{\lambda}\right)},$$

in which Γ is the strength of the vortex, λ is the vortex spacing, and α represents the concentration of vorticity. A larger value of α corresponds to a greater con-

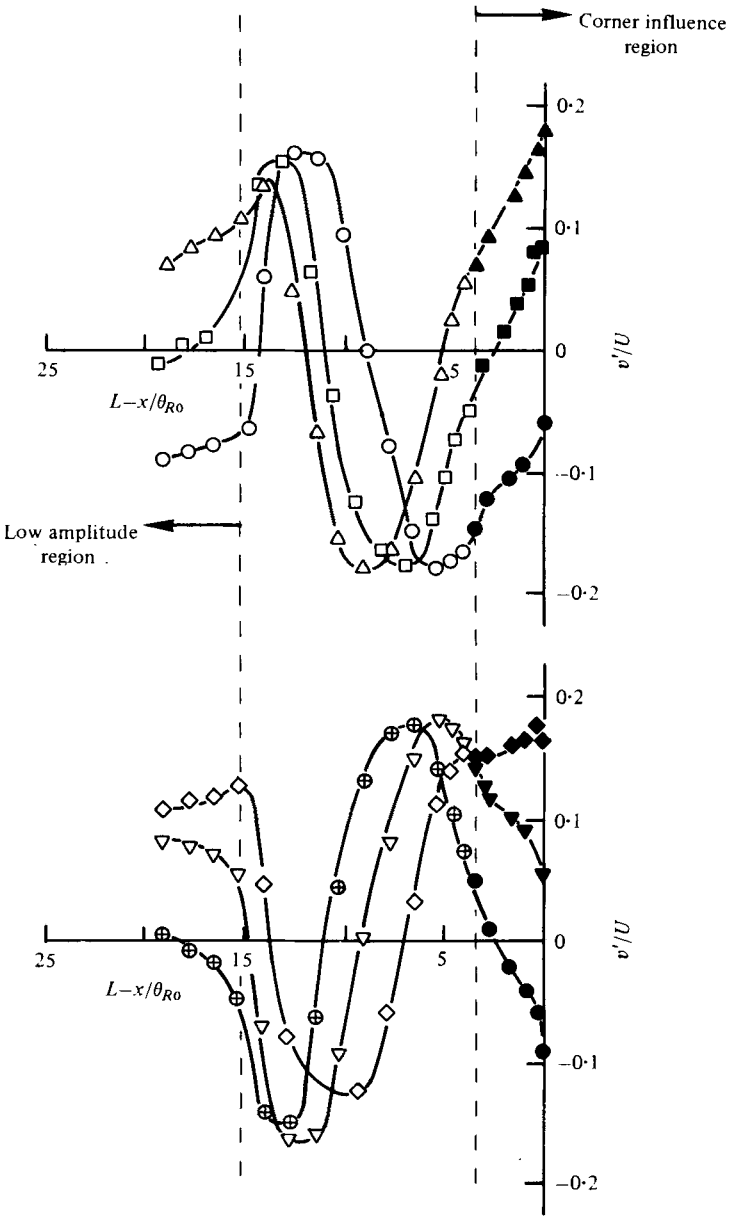

FIGURE 19. Profiles of transverse velocity fluctuation v' as a function of distance from impingement corner $L-x$ at various values of time t/τ. $Re_{\theta_0} = 106$, $L/\theta_0 = 142$, $\epsilon/\theta_{R_0} = 0$. t/τ values are: ○, 0; □, $\frac{1}{8}$; △, $\frac{2}{8}$; ◇, $\frac{3}{8}$; ▽, $\frac{4}{8}$; ⊕, $\frac{6}{8}$.

centration. The case $\alpha = 0$ corresponds to uniform vorticity on lines of constant y, while $\alpha = 1$ represents a row of point vortices. It is evident from the photos of figure 11 that the concentration of vorticity changes in the streamwise direction, so no single value of α is expected to be representative. However, the well-organized nature of the single vortex and the absence of vortex coalescence, which is characteristic of the oscillating cavity flow portrayed in figure 11, provides a better defined case for

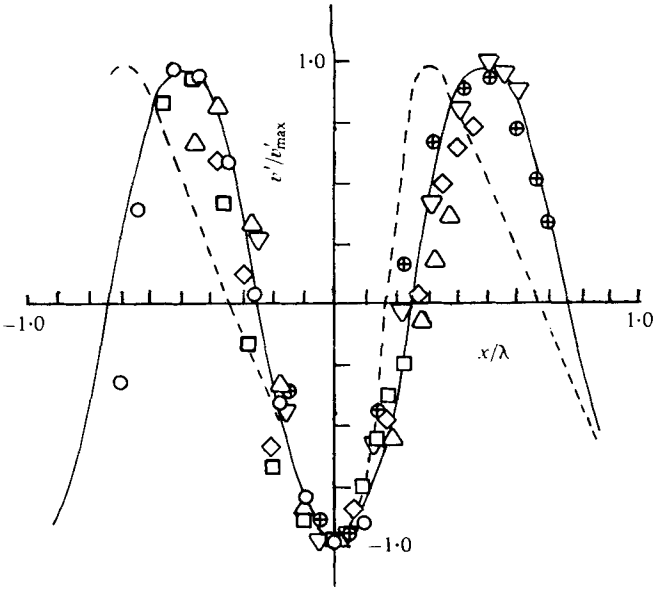

FIGURE 20. Comparison of variations of transverse velocity (see figure 19) with Stuart (1967) model. ——, $\alpha = 0{\cdot}1$; – – –, $\alpha = 0{\cdot}6$.

comparison with the Stuart model than the more complex structure of shear layers involving pairing. Figure 20 shows this comparison for $\alpha = 0{\cdot}1$ and $0{\cdot}6$. In constructing this plot, the six instantaneous profiles of figure 19 (excepting the distortion regions) were referenced (i.e. $x = 0$) with respect to the minimum value of velocity. In general. better agreement is obtained for $\alpha = 0{\cdot}1$. If the vorticity concentration and the amplitude of the transverse fluctuation were invariant with x, all data points of figure 20 would collapse to a single distribution. But the amplitude plots of figure 18 clearly show that this is not the case. In addition, the effects of jitter illustrated in figure 7 may influence the nature of the time-averaged amplitudes of figure 18, and consequently the distributions of figure 19. Such jitter has not been accounted for in the model of Stuart. The severe distortion of the vortex-induced velocity fluctuations upstream of impingement (figure 19) suggests that this region in the immediate vicinity of the impingement edge (within $\sim 4\theta_{R_0}$) should be examined in further detail; in particular, characterization of amplitude and phase of the pressure fluctuations at the corner and their correlation with the distortion of the incident vortex requires study. Such an investigation is currently underway.

6. Conclusions

With the use of a non-invasive method of measurement (laser–Doppler anemometry), it has been shown that the effect of inserting a downstream cavity edge is to markedly alter the spectral evolution of the shear layer in the streamwise direction. This phenomenon has important implications for other configurations of impinging flows – similar enhancement of the organization of the shear layer, relative to the case of no impingement edge, can be expected. The fact that this enhancement is global

in nature, and extends along the entire length of the shear layer, corroborates the hypothesis of disturbance feedback, whereby perturbations are propagated upstream from the impingement surface to the most sensitive (receptive) region of the shear layer near separation. In this regard, further investigations of the impingement geometry and its effectiveness in producing upstream propagating disturbances are called for (Rockwell & Naudascher 1979).

Hydrogen bubble visualization has revealed that the convective speed of a vortex varies with streamwise distance only near the edge; the vortex velocities downstream and sufficiently far upstream of the edge are essentially constant, but have different magnitudes.

Associated with a large amplitude of the transverse velocity fluctuation near the edge is the deformation and possible severing of vortical structures impinging upon the edge. Again, the shape of the impingement edge would seem to be critical; if appropriate alteration of the processes of deformation and severing of impinging structures can be achieved, the amplitude of the locally induced pressure fluctuations should be controllable. In turn, this deformation and severing of structures would seem to be directly tied to the nature of the pressure disturbances which are propagated upstream.

The LDA measurements and hydrogen bubble visualization were carried out while both authors were at the Institute of Hydromechanics, University of Karlsruhe, for the initial phase of the joint research programme 'Flow-induced Vibrations' sponsored by the Volkswagen Foundation. Work subsequent to these experiments was also sponsored by the National Science Foundation. The authors gratefully acknowledge the continuing interest of Prof. E. Naudascher, the advice on LDA measurements given by Prof. F. Durst and Dr R. Kleine, and the insightful critique of the manuscript by Prof. M. V. Morkovin.

REFERENCES

BEARMAN, P. W. 1972 Some measurements of the distortion of turbulence approaching a two-dimensional bluff body. *J. Fluid Mech.* **53**, 451–467.

BROWAND, F. 1966 An experimental investigation of the instability of an incompressible, separated shear layer. *J. Fluid Mech.* **26**, 281–307.

BROWAND, F. K. & WEIDMAN, P. D. 1976 Large scales in the developing mixing layer. *J. Fluid Mech.* **76**, 127–144.

CHANDRSUDA, C., MEHTA, R. D., WEIR, A. D. & BRADSHAW, P. 1978 Effect of free-stream turbulence on large structure in turbulent mixing layers. *J. Fluid Mech.* **85**, 693–704.

DAVIES, P. O. A. L. & YULE, A. J. 1975 Coherent structures in turbulence. *J. Fluid Mech.* **69**, 513–537.

DIMOTAKIS, P. E. & BROWN, G. L. 1976 The mixing layer at high Reynolds number: large structure dynamics and entrainment. *J. Fluid Mech.* **78**, 535–560.

DURST, F., MELLING, A. & WHITELAW, J. H. 1976 *Principles and Practice of Laser–Doppler Anemometry.* London: Academic Press.

FREYMUTH, P. 1966 On transition in a separated laminar boundary layer. *J. Fluid Mech.* **25**, 683–704.

HELLER, H. H. & BLISS, D. 1975 The physical mechanism of flow-induced pressure fluctuations in cavities and concepts for their suppression. *A.I.A.A. Paper* 75-491, *A.I.A.A. 2nd Aero-Acoustics Conf., Hampton, Va., March* 24–26.

HOLDEMAN, J. D. & FOSS, J. F. 1975 The initiation, development, and decay of secondary flow in a bounded jet. *Trans. A.S.M.E.* I, *J. Fluid Engng* **97**, 342–352.

HUSSAIN, A. K. M. F. & ZAMAN, K. B. M. A. 1978 The free shear layer tone phenomenon and probe interference. *J. Fluid Mech.* **87**, 349–383.

KARAMCHETI, K., BAUER, A. B., SHIELDS, W. C., STEGEN, G. R. & WOOLLEY, J. P. 1969 Some basic features of an edge-tone flow field. *Basic Aerodyn. Noise Res., N.A.S.A.* SP-207, *Conf. N.A.S.A. Headquarters, Washington, D.C., July* 14–15, pp. 275–304.

KONRAD, J. H. 1976 An experimental investigation of mixing in two-dimensional turbulent shear flows with applications to diffusion-limited chemical reactions. *Project SQUID Tech. Rep.* CIT-8-PU.

MICHALKE, A. 1965 On spatially growing disturbances in an inviscid shear layer. *J. Fluid Mech.* **23**, 521–544.

MIKSAD, R. W. 1972 Experiments on the nonlinear stages of free shear-layer transition. *J. Fluid Mech.* **56**, 695–719.

POWELL, A. 1961 On the edgetone. *J. Acoustical Soc. America*, **33**, 395–409.

ROCKWELL, D. 1976 Vortex stretching due to shear layer instability. *Trans. A.S.M.E.* I, *J. Fluids Engng* **99**, 240–244.

ROCKWELL, D. & KNISELY, C. 1979 Three-dimensional features of a cavity shear layer. To appear in *Phys. Fluids.*

ROCKWELL, D. & NAUDASCHER, E. 1978 Review – Self-sustaining oscillations of flow past cavities. *Trans. A.S.M.E., J. Fluids Engng* **100**, 152–165.

ROCKWELL, D. & NAUDASCHER, E. 1979 Self-sustained oscillations of impinging free shear layers. *Ann. Rev. Fluid Mech.* **11**, 67–94.

ROCKWELL, D. & NICCOLLS, W. 1972 Natural breakdown of planar jets. *Trans. A.S.M.E.* D, *J. Basic Engng* **94**, 720–730.

ROSHKO, A. 1976 Structure of turbulent shear flows: a new look. *A.I.A.A. J.* **14**, 1349–1357.

SAROHIA, V. 1977 Experimental investigation of oscillations in flows over shallow cavities. *A.I.A.A. J.* **15**, 984–991.

SAROHIA, V. & MASSIER, P. F. 1975 Control of cavity noise. *A.I.A.A. Paper* 75-528, *presented at 3rd A.I.A.A. Aero-Acoustics Conf., Palo Alto, California. July* 20–23.

SONDHAUS, C. 1854 Ueber die beim Ausstroemen der Luft entstehenden Tone. *Ann. Phys. (Leipzig)* **91**, pp. 214–240.

STUART, J. T. 1967 On finite amplitude oscillations in laminar mixing layers. *J. Fluid Mech.* **29**, 417–440.

WINANT, C. D. & BROWAND, F. K. 1974 Vortex pairing: the mechanism of turbulent mixing layer growth at moderate Reynolds number. *J. Fluid Mech.* **63**, 237–255.

Note added in proof. June 1979

A recently completed investigation by the authors shows that ordered cycling between these possible events (figures 7*b*, *c*, *d*) can produce strong components at $0{\cdot}5\beta$ *or* $0{\cdot}4\beta$ *and* $0{\cdot}6\beta$, where β is the fundamental instability frequency; vortex pairing does not occur in any of these cases.